A 4ps Amplitude Reconfigurable Impulse Radiator with THz-TDS Characterization Method in 0.13µm SiGe BiCMOS

Peiyu Chen, Yiqiu Wang, and Aydin Babakhani

Department of Electrical and Computer Engineering, Rice University, Houston, TX 77005, USA

Abstract — This paper reports a fully integrated impulse radiator with the capability of radiating impulses with 4ps FWHM and reconfigurable amplitude. The peak radiated power at 54GHz is 8.7dBm with a 13.6dBm peak EIRP. A Non-Linear Q-Switching Impedance (NLQSI) technique is introduced to generate impulses and control their amplitudes. Furthermore, a two-bit impulse amplitude modulation is achieved through an on-chip four-way impulse combiner, which also attenuates parasitic-induced low-frequency radiation. In addition to performing frequency-domain measurements, for the first time, an ultra-wideband THz Time-Domain Spectroscopy (THz-TDS) system is utilized to characterize the radiated signal in time-domain. The radiated impulse has an SNR>1 bandwidth of more than 160GHz. The fully-integrated impulse radiator is implemented in a 0.13µm SiGe BiCMOS process. It has a die area of 1mm^2 and it consumes 170mW.

Index Terms — BiCMOS, impulse combining, ultra-short impulse radiator, nonlinear Q-switching impedance, THz-TDS.

I. Introduction

Techniques for THz impulse radiation with picosecond FWHM pulse-width and hundreds of GHz bandwidth are in strong demand for wideband spectroscopy, high speed wireless communication, and high resolution imaging [1]. Optical techniques via photoconductive antennas with ultra-fast laser excitations have been widely used in both industry and academia [2], but the high cost of laser-based THz sources limits their use. Recently, laser-free fully-electronic silicon solutions have been reported that produce pulses as short as 8ps. These include an 8ps digital-to-impulse architecture [3], 36ps mm-wave pulse radar [4], and nonlinear transmission lines [5].

In this paper, for the first time, a fully integrated impulse radiator is reported that can radiate impulses with a 4ps Full-Width-Half-Maximum (FWHM) and reconfigurable amplitude. The calculated peak radiated power at 54GHz is 8.7dBm with a measured 13.6dBm peak EIRP. A Non-Linear Q-Switching Impedance (NLQSI) technique is introduced to tune the impulse amplitude. Furthermore, two-bit impulse amplitude modulation is achieved with a four-way impulse combining. In addition, for the first time, an ultra-wideband THz Time-Domain Spectroscopy (THz-TDS) system is utilized to characterize ICs in time-domain, capturing the real time-domain waveform of the radiated 4ps impulse with a record SNR>1 bandwidth of more than 160GHz.

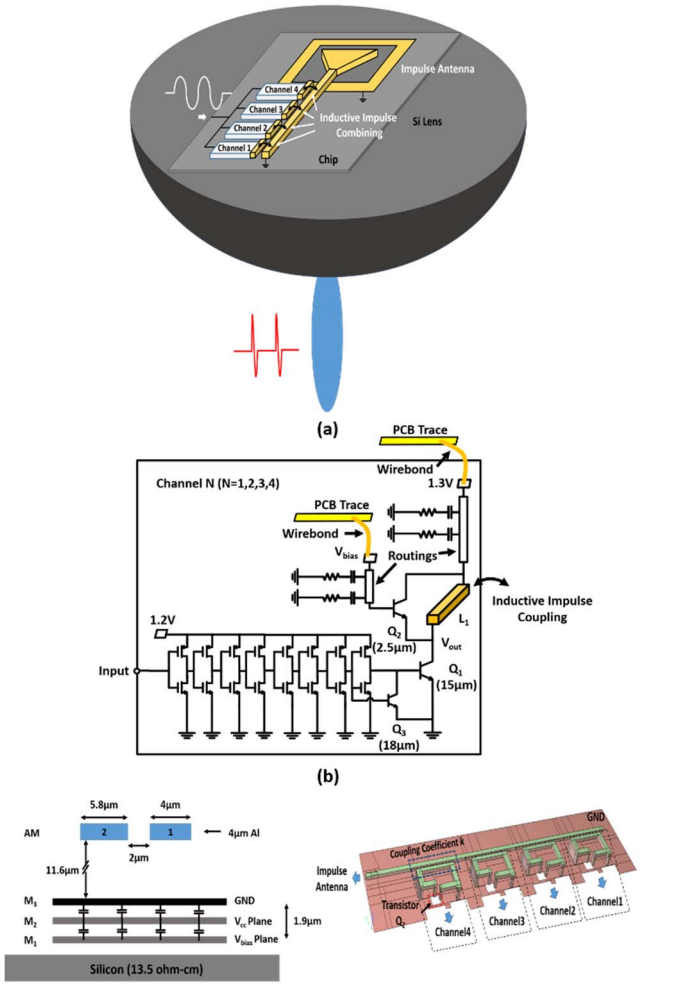

Fig. 1. (a) System architecture of the 4ps impulse radiator. (b) Schematic of a single impulse generation channel. (c) Cross-section of designed impulse combiners and bias routings. (d) 3D structure of the impulse combiner.

II. System Architecture

The reported impulse radiator consists of four impulse generation channels that are combined on-chip (Fig. 1(a)). A 1GHz sinusoidal trigger signal is fed to the chip and distributed to the four channels. As shown in Fig. 1(b), at each channel, an inverter chain transforms the sinusoidal input to a square wave signal, which is directly applied to the base node of switching transistor Q_1. A Bipolar transistor Q_3 is used to

sharpen the falling edges by providing an additional discharge path from Q_1. The first (inductor L_1) and secondary windings of the impulse combiner are implemented on the top metal layer (AM), where the ground layer is implemented on metal layer M3. Metal layers M1 and M2 are used to implement large V_{bias} and V_{cc} planes, respectively, which form a distributed capacitance between them and the ground layer (M3) (Fig. 1(c)). This method provides large parasitic capacitance to ground and enhances the stability of the circuit.

The impulse combiner and bias routings are designed by performing EM simulations (Fig. 1(d)). The inductor L_1 has an inductance of 38pH at 100GHz. The coupling coefficient between inductor L_1 and the secondary winding is 0.58 at 100GHz. The secondary winding is grounded at one end, and the other end is connected to an on-chip, triangle-shaped, microstrip-fed slot impulse antenna. This on-chip antenna is designed to radiate impulses through a high-resistivity silicon lens attached to the backside of the chip [6]. EM simulations are performed by using CST Microwave Studio, HyperLynx 3D EM and HFSS.

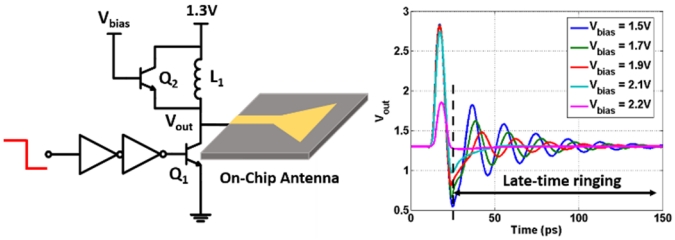

Fig. 2. Simulation results of the Non-Linear Q-Switching Impedance (NLQSI) technique.

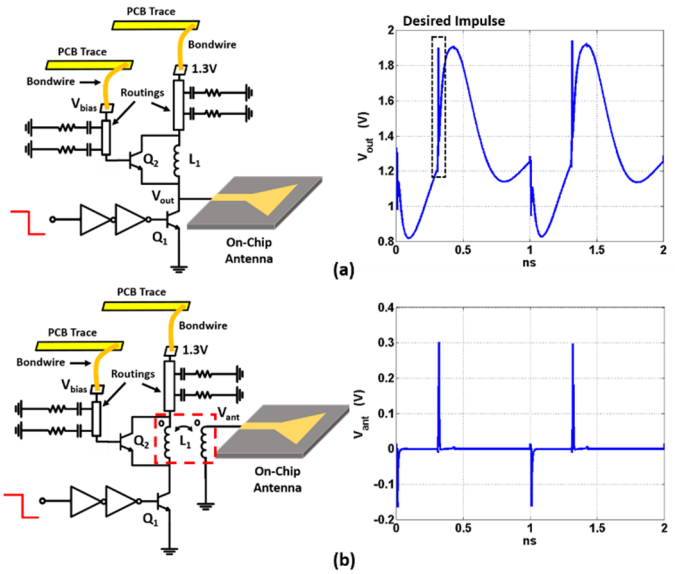

Fig. 3. Simulation results of the impulse coupling scheme.

In each channel, transistor Q_2 enables the NLQSI, which reduces the undesired ringing and tunes the amplitude of the impulse. When transistor Q_1 is switched On by the input trigger signal, a DC current passes through inductor L_1 and transistor Q_1. When the falling edge of the digital trigger signal turns Q_1 off, an impulse waveform is generated at V_{out} with negligible ringing when V_{bias} is close to $V_{cc}+V_{BE(on)}$ (≈2.2V), as shown in Fig. 2. This phenomenon is due to the Q-switching mechanism that NLQSI enables. NLQSI keeps the quality factor (Q) of the resonant load high during impulse generation but reduces Q after impulse generation to minimize the ringing period. In addition, because the peak voltage of the generated impulse is proportional to the Q of the resonant load, it can be varied by the On resistance of transistor Q_2. This effect becomes significant when V_{bias} is larger than 2.1V, which keeps transistor M_2 almost On during the impulse generation period. When V_{bias} is increased from 2.1V to 2.2V, the smaller On resistance of Q_2 decreases the Q of the resonant load, resulting in a reduced peak voltage of the generated impulse (Fig. 2).

Fig. 3 demonstrates the effects of the transmission-line-based impulse coupling scheme. Without the impulse coupling, strong low-frequency ringing appears at the input of the on-chip antenna, V_{ant}, resulting in undesired low frequency radiation. The low-frequency components are caused by the capacitance of the de-Qing blocks and transmission-line effects of on-chip bias routings, wirebonds, and PCB traces (Fig. 3). The de-Qing blocks, consisting of capacitors and resistors in series, are placed along the on-chip bias routings to increase the stability of the circuit. To isolate the strong low-frequency signal from the antenna, a transmission-line-based impulse coupling scheme is implemented. This scheme only couples the high-frequency impulse to the input of the on-chip antenna, as shown in Fig. 3(b). Furthermore, the impulse coupling enables on-chip impulse combining and provides amplitude modulation capability.

III. THz-TDS Time-Domain Characterization

For the first time, a THz-TDS system (Advantest TAS7500TS) is used to characterize the time-domain performance of the reported impulse radiator. The measurement setup is shown in Fig. 4. This system can detect impulses as short as 380fs and provides an SNR>1 bandwidth of more than 4THz. An optical excitation signal from the emitter port is attenuated by a Thorlabs VOA50-APC and then transformed to an electrical trigger signal by a photodetector (Thorlabs DET01CFC). The generated electrical trigger signal is then fed to the impulse radiator. The coherent optical signal from the detector port excites the THz detector module, which samples the received radiated impulse. The sampled and digitized signal is read by a digital oscilloscope (Tektronix 4104B). The measured waveform of the impulse signal, with four impulse generation channels On, and its power spectrum are shown in Fig. 4. The detected impulse has an FWHM of 4ps. Its power spectrum has a 10dB bandwidth of 60GHz and an SNR>1 bandwidth of more than 160GHz.

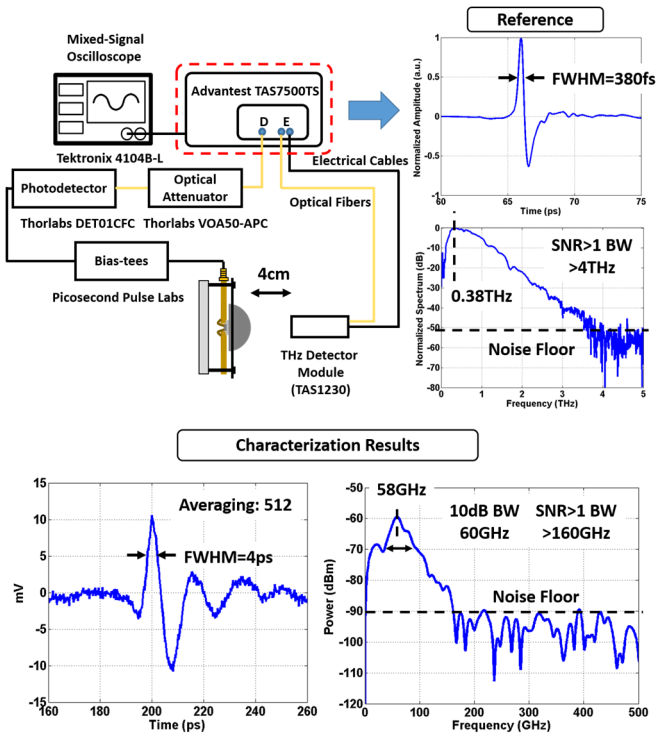

Fig. 4. THz-TDS characterization setup, reference results of the Advantest THz-TDS system, and the measurement results.

IV. Demonstration of Impulse Amplitude Reconfiguration and Impulse Amplitude Modulation

Because the THz-TDS characterization system does not have enough sensitivity to detect low-energy impulses, impulse amplitude modulation is measured by using a custom receiving antenna [3] and a sampling oscilloscope (Keysight 86100D), as shown in Fig. 5(a). As stated in section II, when the NLQSI is fully functioning, i.e. V_{bias} is larger than 2.1V, the tuning effect on the impulse amplitude becomes significant. As observed in the experiment, when V_{bias} is increased from 2.1V to 2.2V, the quality factor of the resonant tank is reduced, resulting in a 0.7mV decrease in the peak amplitude of the impulse (Fig. 5(b)). The ringing effect in the measured waveform is due to the limited bandwidth of the receiving antenna used in this experiment.

Two-bit impulse amplitude modulation is performed by using the same experiment setup. Turning on more impulse generation channels causes the peak amplitude of radiated impulse to increase, as shown in Fig. 5(c). This measurement proves the functionality of the proposed impulse combiner.

V. Frequency-Domain Characterization

In addition to the time-domain measurements, the EIRP spectrum is measured in the frequency domain. To cover the frequency range from 50GHz to 220GHz, four OML spectrum analyzer extension modules are utilized (Fig. 6(a)). Fig. 6(b) reports the measured EIRP spectrum, which peaks at 54GHz.

The measured EIRP spectrum ranges from 50GHz to 197GHz, which is limited by the high loss (~50dB) of the OML mixers in the measurement setup. The measured peak EIRP at 54GHz is 13.6dBm. Measured radiation patterns at 54GHz are shown in Fig. 7. The on-chip antenna has a simulated peak gain of 4.9dBi at 54GHz. As a result, the peak radiated power at 54GHz is calculated to be 8.7dBm.

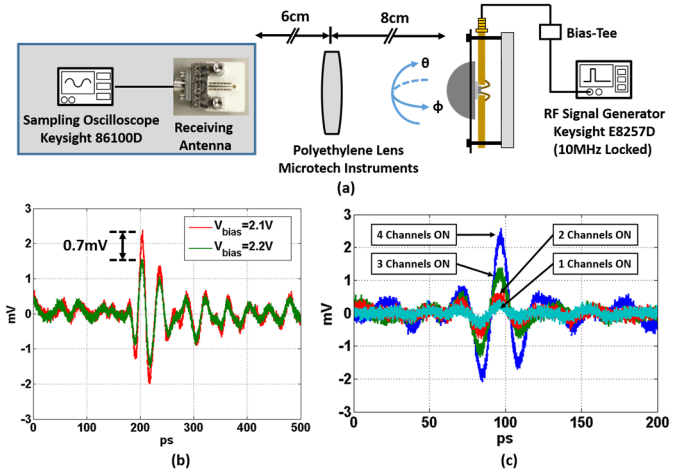

Fig. 5. (a) Measurement setup for demonstrating impulse amplitude modulation. (b) Measured impulse amplitude reconfiguration by NLQSI. (c) Measured two-bit impulse amplitude modulation with more channels enabled.

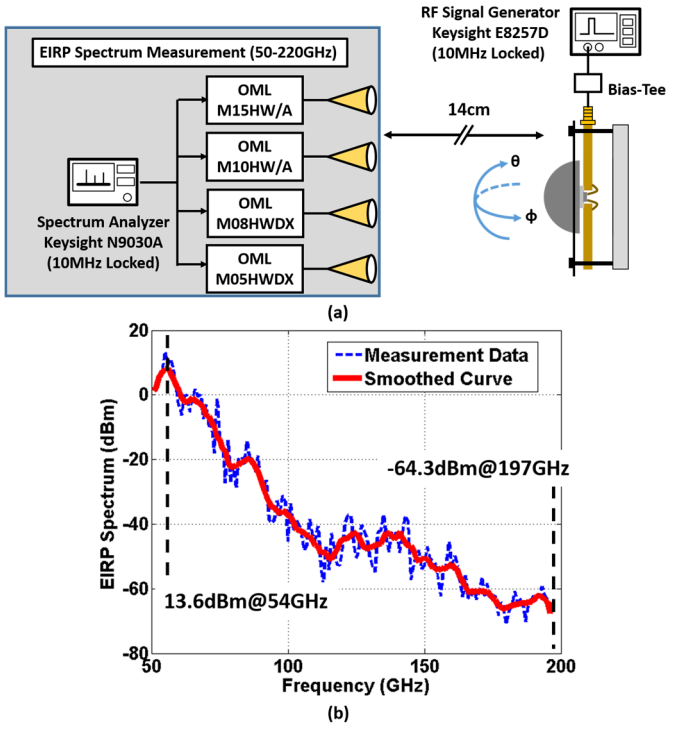

Fig. 6. (a) EIRP spectrum characterization setup for 50-220GHz. (b) Measured EIRP spectrum using a frequency-domain characterization method.

TABLE I
Comparison with state-of-the-art picosecond impulse radiators in silicon

	This Work	[3]	[4]	[5]
Architecture	**Digital-to-Impulse (with NLQSI)**	Digital-to-Impulse	VCO+Modulation	Nonlinear Transmission Line
Pulse Duration (FWHM)	**4ps**	8ps	36ps	N/A
Measured SNR>1 Bandwidth (TD)[1]	**160GHz [1]**	N/A	N/A	N/A
Measured EIRP Spectrum (FD)[2]	**50-197GHz [2]**	50-220GHz	79-109GHz	70-170GHz
Peak EIRP	**13.6dBm @ 54GHz**	13dBm @ 50GHz	N/A	-66dBm @ 160GHz [3]
DC Power	**170mW**	220mW	435mW	N/A [4]
Impulse Amplitude Modulation	**Yes**	No	No	No
THz-TDS Characterization	**Yes**	No	No	No
Technology	**0.13µm SiGe BiCMOS**	0.13µm SiGe BiCMOS	0.13µm SiGe BiCMOS	65nm CMOS+3D Packaging

[1] It is the first work that reports SNR>1 bandwidth measured through the THz-TDS Time Domain (TD) characterization method.
[2] The measured EIRP bandwidth using the Frequency-Domain (FD) setup is limited by the high loss of the harmonic mixers used in the measurement setup.
[3] The measured total radiated power at 10cm distance.
[4] The chip in [5] consists of passive elements and performs pulse shaping without amplification functionality.

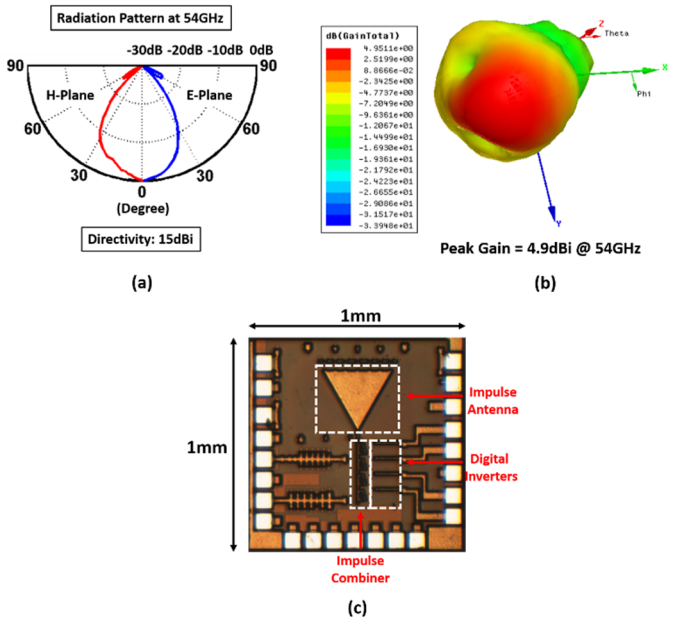

Fig. 7 (a) Measured radiation pattern at the center frequency of 54GHz. (b) Simulated 3D gain pattern of the on-chip antenna at 54GHz (HFSS). (c). Chip Micrograph.

VI. Conclusion

In this paper, a 4ps amplitude reconfigurable impulse radiator is reported. A Non-Linear Q-Switching Impedance (NLQSI) technique is used to generate picosecond impulses. Furthermore, an on-chip impulse combining scheme is introduced to minimize parasitic-induced low-frequency signal radiation. Multiple channels are implemented to increase the power of the radiated impulse and enable two-bit amplitude modulation. For the first time, an ultra-wideband THz-TDS system is used to characterize the chip in time-domain. The chip consumes a DC power of 170mW and occupies a die area of 1mm^2. It is fabricated in a 0.13µm SiGe BiCMOS process. The chip micrograph is shown in Fig. 7(c) and a comparison with current state-of-the-art technology is reported in Table 1.

Acknowledgement

Authors acknowledge Mahdi Assefzadeh for designing the impulse receiving antenna, Eiji Kato for technical supports of the Advantest THz-TDS system, as well as RISC members for valuable discussions. This work is partially funded by the Keck foundation.

References

[1] P. Chen *et al.*, "A 30GHz Impulse Radiator with On-Chip Antennas for High-Resolution 3D Imaging," *IEEE Radio and Wireless Symp.*, Jan. 2015.
[2] P. H. Siegel, "Terahertz technology," *IEEE Trans. Microw. Theory Techn.*, vol. 50, no. 3, pp. 910–928, Mar. 2002.
[3] M. Assefzadeh *et al.*, "An 8-psec 13dBm Peak EIRP Digital-to-Impulse Radiator with an On-chip Slot Bow-Tie Antenna in Silicon, " *IEEE MTT-S Int. Microwave Symp.*, Jun. 2014.
[4] A. Ababrian *et al.*, "A 94GHz mm-Wave-to-Baseband Pulse-Radar Transceiver with Applications in Imaging and Gesture Recognition," *IEEE J. of Solid-State Circuits*, vol. 48, no. 4, pp. 1055-1071, Apr. 2013.
[5] L. Tripodi *et al.*, "Broadband CMOS Millimeter-Wave Frequency Multiplier with Vivaldi Antenna in 3-D Chip-Scale Packaging," *IEEE Trans. Microw. Theory Techn.,* vol. 60, no. 12, pp.3761-3768, Dec. 2012.
[6] A. Babakhani *et al.*, "A 77-GHz Phased-Array Transceiver with On-Chip Antennas in Silicon: Receiver and Antennas," *IEEE J. of Solid-State Circuits*, vol. 41, no. 12, pp. 2795-2806, Dec. 2006.